Int J Adv Manuf Technol (2016) 86:407–418
DOI 10.1007/s00170-015-8181-0

ORIGINAL ARTICLE

Modeling study on surface roughness of ultrasonic-assisted micro end grinding of silica glass

Zhang Jian-hua[1] · **Wang Li-ying**[1] · **Tian Fu-qiang**[1] · **Zhao Yan**[1] · **Wei Zhi**[1]

Received: 17 August 2015 / Accepted: 24 November 2015 / Published online: 11 December 2015
© Springer-Verlag London 2015

Abstract Ultrasonic vibration-assisted micro end grinding (UAMEG) is a promising processing method for microparts made of hard and brittle materials. The surface quality of the workpiece in UAMEG is important, as it influences the performance of the finished part to a great extent. However, the surface finish is governed by many factors, and its experimental determination is laborious and time-consuming. So, it is a key issue to establish a model for the reliable prediction of surface roughness in UAMEG. In this paper, a new analytical surface roughness model is developed considering the influence of random distribution of abrasives, grinding conditions, and ultrasonic vibration, which shows the relationship between the surface roughness and the expected value of chip thickness, based on the assumption that the profile of groove produced by an individual grain is a triangular shape. This model is validated by the experimental results of silica glass in UAMEG. The theoretical predicted value of surface roughness matches well with the experimental result.

Keywords Ultrasonic vibration · Microgrinding · Hard and brittle materials · Surface roughness · Chip thickness

✉ Zhang Jian-hua
jhzhang@hebut.edu.cn

Wang Li-ying
lywangedu@sina.com

Tian Fu-qiang
fqtianhebut@126.com

Zhao Yan
zhaoyan5995@gmail.com

Wei Zhi
weiwhizz@hebut.edu.cn

[1] School of Mechanical Engineering, Hebei University of Technology, Tianjin 300132, China

1 Introduction

In recent years, rapid development of micromachining technology has been promoted by expanding requirements of microproducts, such as microoptical system and microrobot [1, 2]. Meanwhile, hard and brittle materials, such as glass and ceramics, exhibit many excellent properties: high hardness; superb dimensional stability; high mechanical strength; and prominent thermal, chemical, and wearing resistance [3, 4]. These properties make them suitable material for manufacturing of precision components. But, these properties of hard and brittle materials make them difficult to cut. In the conventional machining conditions, the chip formation is usually a fracture process that damages the machined surface and leads to unacceptable part quality [5]. To introduce ultrasonic vibration into machining process has been proved to be a promising method that could significantly improve machining surface quality, as well as decrease machining force and heat, increase critical cutting depth of the brittle-ductile removal transition, and prolong tool life [6]. Tawakoli and Bahman [7] conducted comparative experiments of ultrasonic-assisted dry grinding and conventional dry grinding of 42CrMo4, which demonstrated considerable advantages of the former technology, significant improvement on the R_z parameter, up to 60 % reduction of normal grinding force. Similar comparative experiments were conducted on 100Cr6 [8], and the results indicate that the added ultrasonic vibration contributes to considerable elimination of the workpiece surface and subsurface thermal damage, increase of the G-ratio, and decrease of the grinding forces. Chen [9] conducted an experimental study of the effects of ultrasonic vibration on grinding surface roughness, showing that the application of ultrasonic vibration to the grinding process can lower the workpiece surface roughness. In Yan's research [10], comparative grinding experiments on surface quality of nano-ZrO2 ceramic were carried out using

diamond wheel in different condition, both with and without ultrasonic vibration. The results show that the surface quality is improved with ultrasonic assistance compared with conventional diamond grinding. In addition, it is easier for ultrasonic-assisted grinding to achieve material ductile region removal. In the Prasanna et al.'s [11] study on force and thermal effects in vibration-assisted grinding, experiments of dry and wet grinding as vibration frequency below ultrasonic were conducted. Reductions in force of up to 30 % and in heat flux into workpiece up to 42 % are observed for dry grinding with ultrasonic assistance. J. Can and X. Wang [12] applied ultrasonic vibration to single-crystal diamond tool tip in turning fused silica and achieved ductile machining (surface roughness was 100 nm) with depth of cut 2 μm as a significant increase in the critical depth of cut. In the previous work of Zhang and Zhao, experiment of ultrasonic-assisted micro end grinding of silica glass was conducted by Lin to study the effect of ultrasonic vibration on grinding force and surface quality [12, 13]. The results indicate that the surface quality is significantly improved and grinding forces are significantly reduced due to ultrasonic vibration. But, the mechanism of influence of grinding parameters and ultrasonic vibration on surface quality in UAMEG is meanly studied experimentally and primarily. Further research on modeling of surface roughness is important and necessary to UAMEG.

The complete description of the surface generated by grinding is very difficult due to the complex behavior of different grains producing grooves because of the random grain-work interaction. In previous studies, several analytical models, based on stochastic nature of grinding process, were proposed to simulate the surface profile generated during grinding. Hecker [14] presented a mathematical model of surface roughness in cylindrical grinding based on a probabilistic undeformed chip thickness model, Rayleigh's probability density function, in which the wheel microstructure and the material properties were considered. The grooves left on the surface by ideal conic grains are geometrically analyzed. By introducing a correction factor into the surface roughness model, the average error between predictive results and experimental results is proved to be 10 %. Using the Rayleigh's probability density function to describe the undeformed chip thickness, Agarwal [15] developed an analytical model of surface roughness in ceramic grinding, which shows a proportional relationship between the surface roughness and the chip thickness expected value, based on the assumption that groove produced by an individual grain to be an arc of a circle. Agarwal [16] conducted further research on surface roughness modeling in ceramic grinding. The cross section of the groove produced by an individual grain is assumed to be parabolic in shape. In addition, an overlap factor is introduced to define the influence of area lost due to grooves overlapping on surface roughness. Gao [17] created a theoretical model of surface roughness for ultrasonic vibration cylindrical grinding on nano-zirconia ceramics. Considering the total interfering times of adjacent two grain traces, model of interval between two adjacent grain traces was developed. Then, the model of theoretical maximal value of surface roughness was established based on geometry of ultrasonic vibration grinding. In Gopal's [18] study on silicon carbide cylindrical grinding, a new chip thickness model was developed to predict the surface quality. Then, a surface roughness model incorporating the modulus of elasticity of the grinding wheel and the elastic deformation of the workpiece was established and validated by experiments. However, the surface finish in UAMEG is still unclear; the influence of ultrasonic vibration on the surface roughness of the grinding is not very explicit.

In this paper, an analytical model is built, incorporating the effect of overlapping of triangular-shaped grooves, to evaluate surface roughness from the chip thickness probability density function. The material properties, the wheel microstructure, the kinematic grinding conditions, etc. are included in this model. The model of surface roughness is based on a probabilistic analysis, where the main random variable is the chip thickness, the center-to-center distance between adjacent two grooves, and internal angle (2θ) of the cone. The relationship between the surface roughness and the undeformed chip thickness is found, which can be used to predict the surface roughness. The verification experiment is conducted under different levels of ultrasonic amplitudes, wheel speeds, and grinding depths. The predicted and the measured values of surface roughness are in very good agreement.

1.1 Surface formation process in UAMEG

The surface formation process in UAMEG is very important to establish a reasonable surface roughness prediction model. The surface formation is introduced in this section.

Figure 1a shows the coordinate system of UAMEG in this paper. The x axis is in the precision feed direction of grinding wheel, along which the workpiece operates simple harmonic motion with small amplitude and high frequency. The y axis is oriented in cross-feed direction. The z axis is normal to uncut workpiece surface and is the direction of cutting depth, around which the grinding wheel rotates at high speed. Several hypothesis conditions in grinding process are put forward for this study: abrasives are well-distributed with uniform size; deformation and run out of the wheel are negligible; and the wheel end face is parallel to workpiece surface, ultrasonic amplitude, and frequency keep steady in machining process.

From Fig. 1a, it can be seen that exterior margin abrasives on grinding wheel end face firstly cutting into the unmachined material, leading to shearing-forming chip under specific cutting depth and other processing parameters; inner margin abrasives only encounter the machined material, which mainly lead to sliding, plough, and repeatedly ironing to the

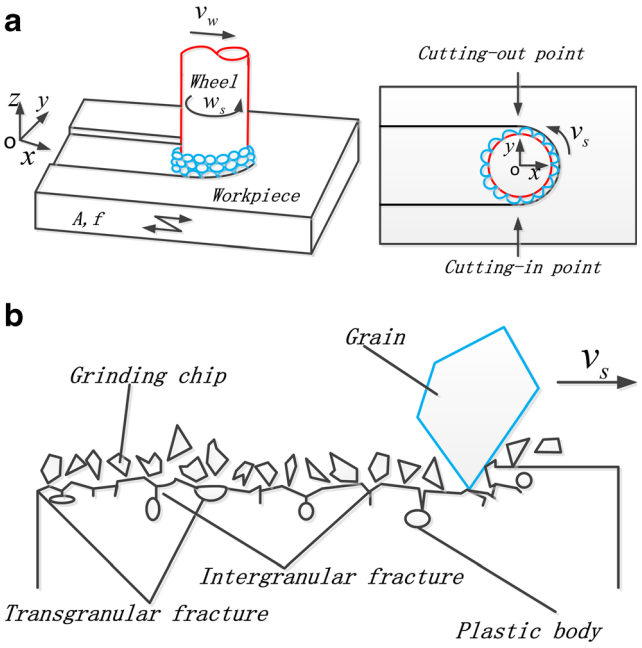

Fig. 1 Surface formation process in UAMEG. **a** Coordinate system. **b** Surface formation

machined material surface generated by former abrasives due to springback.

Figure 1b shows the surface formation mechanism of UAMEG. It can be seen approximately as materials continuously extruded, scratched by grain, which result in lateral crack of different depths and intermittent median crack. Due to crack bridge, lateral crack continually propagates and results in microcrack network. Indentation which occurs on the new surface resulted from grinding chip formation. Surface planeness occurs on the new surface, which is attributed to overhang occurred instant local brittle fracture under the scratch (transgranular fracture). Crack propagation is blocked by plastic zones inside materials of random distribution. As a result, plastic zone removal mode is formed due to plastic component on the surface under the grain scratch. The surface formation process is made easier because of the high-frequency interaction between the active grits and the rapid acceleration of the workpiece. The chips are cut away more easily. Due to the oscillating impacts between the grits and the workpiece, the microcracks in the contact zone can spread more quickly and have a positive effect on the next process of chip formation.

In summary, powdery chips are formed in the machining process of UAMEG. The surface is formed by the coexistence mechanism of brittleness and ductility under the scratching effect of abrasives. Due to a large proportion of the ductility and the complexity of the mechanism of brittleness, the influence of brittle material fracture on surface roughness is ignored in this paper.

1.2 Modeling of surface roughness in UAMEG

In this section, an analytical model is built, incorporating the effect of overlapping of triangular-shaped grooves, to evaluate surface roughness from the chip thickness probability density function. The surface roughness model is developed considering the influence of random distribution of abrasives, grinding conditions, and ultrasonic vibration. The overlapping effect is characterized by the center-to-center distance between adjacent two grooves defined as h. There are three variables in the model, respectively, chip thickness, the center-to-center distance between adjacent two grooves, and internal angle (2θ) of the cone. First of all, according to the definition of R_a, the centerline is computed. Then, considering the overlapping effect, the model is developed. Finally, to validate the correctness of the model, the value of the variable is calculated.

1.2.1 Surface roughness calculation

To take account of random distribution of abrasives on wheel surface, Rayleigh's probability density function [19], which describes the undeformed chip thickness t, is introduced to describe the surface roughness model.

$$f(t) = \begin{cases} \left(t/\beta^2\right) e^{-\left(t^2/2\beta^2\right)} & \text{for } t \geq 0 \\ 0 & \text{for } t < 0 \end{cases} \quad (1)$$

where β is a parameter that completely defines the probability density function, which depends on the cutting conditions, microstructure of the grinding wheel, the properties of workpiece material, etc.

The expected value of this function can be expressed as

$$E(t) = \left(\sqrt{\pi/2}\right)\beta \quad (2)$$

The surface roughness, R_a, can be calculated using the chip thickness probability density function defined in Eq. (1). But, there are actually many tiny cutting points on an individual grain surface, and the profile of the grain is irregular because of the random grain-work interaction. So, some assumptions are made in this work for simplicity:

(1) The groove produced by an individual grain is assumed to be of a triangular shape that comes from the projection of the assumed conical shape for grains.
(2) The groove shape is described by the internal angle (2θ) of the cone and chip thickness t as shown in Fig. 2. All grooves are characterized by the same internal angle but varying chip thickness t.
(3) It is assumed that the plowing effect with pileup and the influence of brittle material fracture on surface roughness are ignored.

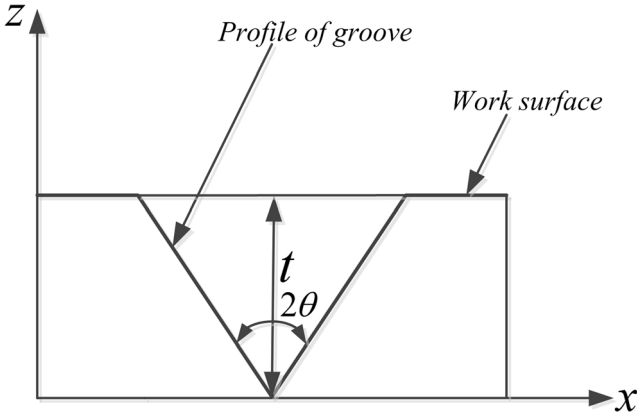

Fig. 2 Sectional view showing the shape of groove generated

(4) The overlapping effect of adjacent two grooves is incorporated for effective modeling of surface roughness in this work.

The surface roughness, R_a, is defined as the arithmetic average of the absolute values of the deviations of the surface profile height from the mean line within the sampling length. So, the surface roughness R_a can be expressed as

$$R_a = \frac{1}{l}\int_0^l |z - z_m| dl \tag{3}$$

where z_m donates the distance of the centerline, which is drawn in such a way based on the definition of R_a that the areas above and below it are equal, as is shown in Fig. 3. Define $P(z)$ as the probability that the height of grain has a particular value z. Then, R_a can be expressed as

$$R_a = \frac{1}{l}\int_{z_{\min}}^{z_{\max}} |z - z_m| p(z) dz \tag{4}$$

where $z_{\max}$ and $z_{\min}$ are the lowest and highest peak height of the surface profile.

According to the definition of the centerline z_m, during the abrasive-workpiece interaction in UAMEG, two types of grooves are generated depending on their depth of engagement is either less or greater than centerline z_m, as shown in Fig. 3. According to the definition of R_a, the area above and below the centerline must be equal. So, the expected value of total area can be expressed as

$$E\{A(t)\} = 0 \tag{5}$$

Incorporating the probability density function of undeformed chip thickness $f(t)$, expected value of total area can be deduced to be

$$\int_0^\infty A(t) f(t) dt = 0 \tag{6}$$

For the groove with the depth of engagement less than z_m, the expected value of area A_1 contributing to surface roughness can be expressed as

$$E\{A(t_1)\} = \int_0^{z_m} A(t_1) f(t) dt = \int_0^{z_m} A_1 f(t) dt \tag{7}$$

For the groove with depth of engagement greater than z_m, expected value of area A_2 can be expressed as

$$\begin{aligned} E\{A(t_2)\} &= \int_{z_m}^\infty A(t_2) f(t) dt \\ &= \int_{z_m}^\infty \left(A_2^{\text{upper}} - A_2^{\text{lower}}\right) f(t) dt \end{aligned} \tag{8}$$

By substituting the values from Eqs. (7) and (8) to Eq. (6), it can be rewritten as

$$\int_0^{z_m} A_1 f(t) dt + \int_{z_m}^\infty \left(A_2^{\text{upper}} - A_2^{\text{lower}}\right) f(t) dt = 0 \tag{9}$$

or

$$P_1 E(A_1) + P_2\left[E\left(A_2^{\text{upper}}\right) - E\left(A_2^{\text{lower}}\right)\right] = 0 \tag{10}$$

where P_1 and P_2 are, respectively, defined as the probability that the depth of abrasive-workpiece engagement is either less and greater than centerline z_m and are expressed as

$$P_1 = \int_0^{z_m} f(t) dt = 1 - e^{-z_m^2/2\beta^2} \quad for\ t < z_m \tag{11}$$

$$P_2 = \int_{z_m}^\infty f(t) dt = e^{-z_m^2/2\beta} \quad for\ t > z_m \tag{12}$$

According to geometrical relationship in Fig. 3, the expected value of the area of the groove with engagement depth less

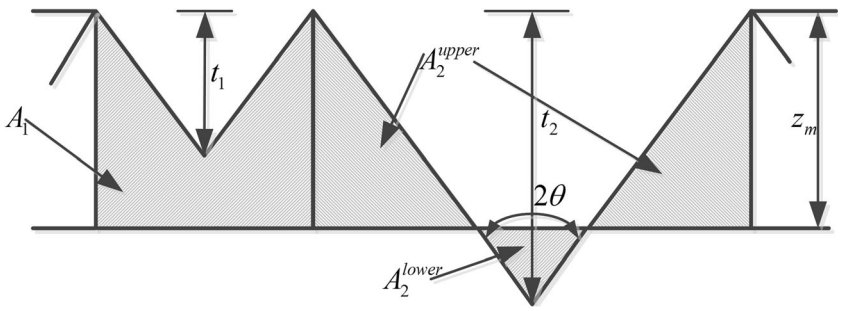

Fig. 3 Profile of grooves generated

than centerline contributing to surface roughness R_a can be expressed as

$$E(A_1) = 2z_m\tan\theta E(t_1) - \tan\theta E\left(t_1^2\right) \tag{13}$$

where A_1 is the intercepted area between abrasive profile and the centerline contributing to surface roughness.

Similarly, the expected value of the area of the groove with engagement depth greater than the centerline contributing to surface roughness can be calculated as

$$E\left(A_2^{\text{upper}}\right) = \frac{1}{2}z_m^2\tan\theta \tag{14}$$

$$E\left(A_2^{\text{lower}}\right) = \tan\theta\left(E\left(t_2^2\right) - 2z_m E(t_2) + z_m^2\right) \tag{15}$$

where $A_2{}^{\text{upper}}$ and $A_2{}^{\text{lower}}$ are the areas above and below the centerline. After substituting the expected values from Eqs. (13), (14), and (15), Eq. (10) can be rewritten as

$$2z_m(p_1E(t_1) + p_2E(t_2)) = p_1E\left(t_1^2\right) + p_2E\left(t_2^2\right) \tag{16}$$

For the abrasives having engagement depth lying between 0and z_m, the probability density function of the chip thickness will be given by the conditional probability density function as

$$f_1(t) = f_1(t|0 \le t < z_m) = \frac{f(t)}{\int_0^{z_m} f(t)dt} \tag{17}$$

For the abrasives with engagement depth above z_m, the conditional probability density function can be given as

$$f_2(t) = f_2(t|z_m \le t < \infty) = \frac{f(t)}{\int_{z_m}^{\infty} f(t)dt} \tag{18}$$

Substitute Eqs. (17) and (18) to Eq. (16) for calculation of z_m. After simplification, z_m can be expressed as

$$z_m = \frac{1}{2}\left(\frac{E(t^2)}{E(t)}\right) \tag{19}$$

$E(t)$ and $E(t^2)$ can be calculated to be

$$E(t) = \sqrt{\frac{\pi}{2}}\beta \tag{20}$$

$$E\left(t^2\right) = 2\beta^2 \tag{21}$$

Then, z_m can be given as

$$z_m = \sqrt{2/\pi}\beta \tag{22}$$

The overlapping effect can be characterized by the center-to-center distance between adjacent two grooves defined as h, as shown in Fig. 4. It is assumed in this paper that a groove can only be overlapped by the groove with the same chip thickness. Then, the expected value of the area of the two adjacent grooves with engagement depth less than centerline contributing to surface roughness R_a, considering the overlapping effect, can be expressed as

$$A_1^{'} = (2t_1\tan\theta + h)(z_m - t_1) + t_1^2\tan\theta + \frac{h^2}{4\tan\theta} \tag{23}$$

Similarly, for the groove with depth of engagement greater than z_m, the areas below and above the centerline after overlapping can be, respectively, expressed as

$$A_{2\text{upper}}^{'} = z_m^2\tan\theta \tag{24}$$

$$A_{2\text{lower}}^{'} = 2\tan\theta(t_2 - z_m)^2 - \tan\theta\left(t_2 - z_m - \frac{h}{2\tan\theta}\right)^2 \tag{25}$$

Considering the difference of contribution of the two types of grooves below and above the centerline, total expected value of surface roughness considered overlapping factor can be expressed as

$$E(R_a) = p_1E(R_{a1}) + p_2E(R_{a2}) \tag{26}$$

The probability that the undeformed chip thickness value t is smaller than the centerline position, z_m, can be calculated as

$$P_1 = \int_0^{z_m} f(t)dt = 1 - e^{-z_m^2/(2\beta^2)} \tag{27}$$

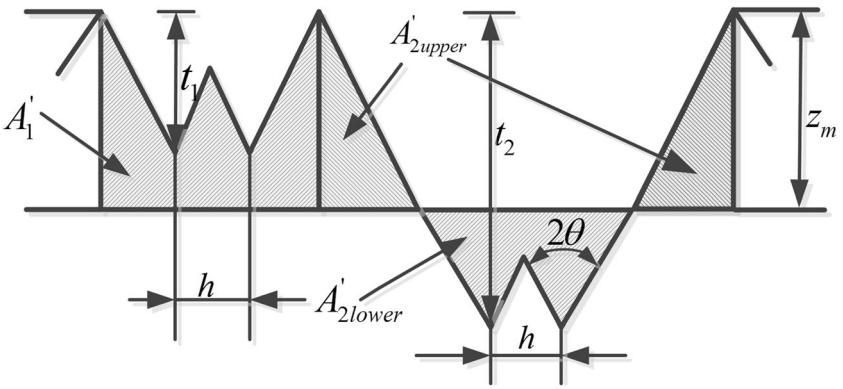

Fig. 4 Profile of grooves generated

Then, according to the definition of probability density function, the probability of the undeformed chip thickness above the centerline position, z_m, can be expressed as

$$P_2 = 1-P_1 = e^{-z_m^2/(2\beta^2)} \tag{28}$$

The influence of center-to-center distance between adjacent two grooves h on the total groove profile length is ignored. Then, the expected values of surface roughness for these two types of grooves can be, respectively, written as

$$E(R_{a1}) = E\left(\frac{A_1'}{4\,t_1\tan\theta}\right) \tag{29}$$

$$E(R_{a2}) = E\left(\frac{A_{2\text{upper}}' + A_{2\text{lower}}'}{4t_2\tan\theta}\right) \tag{30}$$

By substituting Eqs. (23), (24), and (25) to Eqs. (29) and (30), $E(R_{a1})$ and $E(R_{a2})$ can be rewritten as

$$E(R_{a1}) = \frac{z_m}{2} - \frac{E(t_1)}{4} + \frac{E\left({}^{1}/_{t_1}\right)E(h)(z_m - t_1)}{4\tan\theta} + \frac{E\left({}^{1}/_{t_1}\right)E(h^2)}{16\tan^2\theta} \tag{31}$$

$$E(R_{a2}) = \frac{z_m^2 E\left({}^{1}/_{t_2}\right)}{2} + \frac{E(t2)}{4} - \frac{z_m}{2} + \frac{E(h)}{4\tan\theta} - \frac{z_m E(h) E\left({}^{1}/_{t_2}\right)}{4\tan\theta} - \frac{E\left({}^{1}/_{t_2}\right)E(h^2)}{16\tan^2\theta} \tag{32}$$

Similar to Agarwal's [11, 12] research, $E(t_1)$ and $E(t_2)$ can be deduced and given as a function of β:

$$E(t_1) = 0.51\beta \tag{33}$$

$$E(t_2) = 1.53\beta \tag{34}$$

$E(1/t_1)$ and $E(1/t_2)$ can be deduced as follows:

$$E\left({}^{1}/_{t_1}\right) = \frac{1}{P_1}\int_0^{z_m}\frac{1}{t}f(t)dt = \frac{\sqrt{2}}{2P_1\beta}\left(\sqrt{\pi}\,\mathrm{erf}\left(\frac{z_m}{\sqrt{2}\beta}\right)\right) = 2.64\frac{1}{\beta} \tag{35}$$

$$E\left({}^{1}/_{t_2}\right) = \frac{1}{P_2}\int_{z_m}^{+\infty}\frac{1}{t}f(t)dt = \frac{\sqrt{2}}{2P_2\beta}\left(\sqrt{\pi}\left(1-\mathrm{erf}\left(\frac{z_m}{\sqrt{2}\beta}\right)\right)\right) = 0.75\frac{1}{\beta} \tag{36}$$

According to Eq. (2), β can be expressed by the expected value of chip thickness $E(t)$ as

$$\beta = 0.798E(t) \tag{37}$$

Substitute Eqs. (31), (32), (33), (34), (35), (36), and (37) and Eqs. (27) and (28) into Eq. (26), then the total expected value of surface roughness can be given as

$$E(R_a) = 0.188E(t) + \frac{0.125E(h)}{\tan\theta} + \frac{0.014E(h^2)}{\tan^2\theta E(t)} \tag{38}$$

Then, the surface roughness model is developed considering the influence of random distribution of abrasives, grinding conditions, and ultrasonic vibration, which shows a relationship between the surface roughness and the expected value of chip thickness, based on the assumption that the profile of groove produced by an individual grain is a triangular shape.

1.3 Expected value of chip thickness $E(t)$

The chip thickness modeling plays a major role in prediction of surface roughness. In this section, expected value of chip thickness is calculated based on the static cutting density model developed by Hacker, which is given as

$$C_s = A_s Z^{k_s} \tag{39}$$

where C_s is the static cutting density, Z is the depth into the wheel, and A_s and k_s are the coefficients characterizing the wheel topography.

In this work, the chip thickness for a given grain is defined as the difference of its height of protrusion and the maximum height of protrusion of all grains on wheel end face. Then, based on the definition of static cutting density, distribution function of chip thickness can be defined as

$$C(t) = \begin{cases} 0 & (t\in(-\infty\ ,\ 0)) \\ \dfrac{A_s\ t^{k_s}}{A_s\ t_{\max}^{k_s}} & (t\in[0\ ,\ t_{\max}]) \\ 1 & (t\in(t_{\max}\ ,\ +\infty)) \end{cases} \tag{40}$$

In Park's [20] research, the wheel topography of an electroplated carbon boron nitride (CBN) wheel with 230~270 grit number was experimentally analyzed using a microscope to extract the profile of the microgrinding wheel. The grain sizes for a wheel in the range of 230~270 fall in the range of 39 to 47 μm. The maximum feasible chip thickness is assumed to be the one third of maximum value of grain size 47 μm. For fresh tool, A_s and k_s are, respectively, calculated to be 2.355 and 0.922 and for worn tool 2.211 and 0.8527. In this work, the average values of A_s and k_s for fresh tool and worn tool are adopted to calculate the expected value of chip thickness. $f'(t)$ is defined as the probability density function of chip thickness and can be given as

$$f'(t) = \begin{cases} 0 & (t\in(-\infty,\ 0)) \\ \dfrac{A_s k_s t^{k_s-1}}{A_s \times t_{\max}^{k_s}} = 0.077t^{-0.1126} & (t\in[0, 15.67]) \\ 0 & (t\in(15.67,\ +\infty)) \end{cases} \tag{41}$$

In this work, experiments are conducted under four levels of grinding depths of 1, 1.5, 2, and 2.5 μm. The expected value of chip thickness under these four conditions can be deduced as follows:

$$E(t)_{ap_i} = \int_0^{ap_i} t f'(t)dt \quad (ap_i = 1, 1.5, 2, 2.5 \quad \text{for } i = 1, 2, 3, 4) \tag{42}$$

The expected values of chip thickness under those four levels of grinding depth calculated using Eq. (41) are shown in Table 1.

1.4 Modeling of the center-to-center distance between adjacent two grooves *h*

In order to modally incorporate the effect of overlapping interaction of abrasives on surface roughness, model of the center-to-center distance between adjacent two grooves h is established in this section; the geometrical schematic is shown in Fig. 5.

The time when the former abrasive (here defined as the (i)th abrasive) moves to point Q and the cutting abrasive (here defined as the $i + 1$th abrasive) moves to point N is defined as the start time. t_B is defined as the time when the ith abrasive moves to point B (x_{tB}, y_{tB}) along the dashed line. At the same time, the center of the wheel moves to point O_i. Point A (x_{tA}, y_{tA}) is the intersection of trajectory of the ($i + 1$)th abrasive and the extension line of l_{BOi}. The ($i + 1$)th abrasive moves to point A at t_A, and the center of the wheel moves to point O_{i+1} at the same time.

Based on geometrical relationship in Fig. 5, center-to-center distance between the adjacent two grooves generated by the ith and the ($i + 1$)th abrasives at t_A can be expressed as

$$h_{i+1}^{t_A} = \sqrt{r^2 + L^2 - 2rL\cos[\omega_s(t_A - \Delta_t)]} - r \tag{43}$$

where Δ_t ($\Delta_t = 1/mn$) is defined as the time difference according to the phase difference of these two adjacent abrasives, which is equal to the time that the ($i + 1$)th abrasive moves from point N to point M; m is the quantity of all the abrasives in the most exterior margin of microwheel end face, n is the spindle speed, and L is the distance between O_i and O_{i+1}.

$$L = x_{0_{i+1}} - x_{o_i} \tag{44}$$

Table 1 The expected values of chip thickness

i	ap_i (μm)	$E(t)$ (μm)
1	1	0.040
2	1.5	0.087
3	2	0.150
4	2.5	0.228

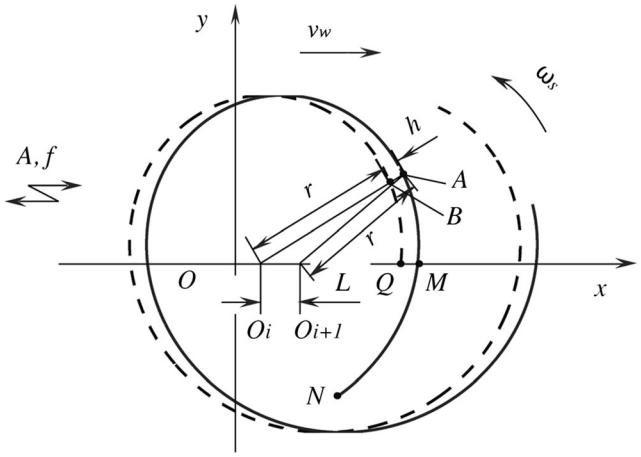

Fig. 5 Geometrical schematic of center-to-center distance between adjacent two grooves

where $x_{O_i}^{t_B}$ and $x_{O_{i+1}}^{t_A}$ are the x position of the wheel center at t_B and t_A, respectively, which can be further expressed as

$$\begin{cases} x_{O_{i+1}}^{t_A} = v_w \cdot t_A + A \cdot \sin(\omega_f \cdot t_A) \\ x_{O_i}^{t_B} = v_w \cdot t_B + A \cdot \sin(\omega_f \cdot t_B) \end{cases} \tag{45}$$

Then, the line l_{BOi} can be given as

$$l_{BO_i} : y_{t_B} = \left(x_{t_B} - x_{O_i}^{t_B}\right) \tan(\omega_s \cdot t_B) \tag{46}$$

The trajectory of the ($i + 1$)th abrasive in UAMEG can be expressed by

$$\begin{cases} x_{i+1} = v_w t + r\cos(\omega_s(t - (i+1)\Delta_t)) + A\sin(\omega_f t) \\ y_{i+1} = r\sin(\omega_s(t - (i+1)\Delta_t)) \end{cases}, (i = 0, 1, 2\ldots) \tag{47}$$

where ω_f ($\omega_f = 2\pi f$) is the angular frequency of ultrasonic vibration.

Because the point A (x_{tA}, y_{tA}) is the intersection of the trajectory of the ($i + 1$)th abrasive and the extension line of l_{BOi}, the following simultaneous equations system can be derived:

$$\begin{cases} x_{t_A} = v_w \cdot t_A + r \cdot \cos(\omega_s \cdot (t_A - \Delta_t)) + A \cdot \sin(\omega_f \cdot t_A) \\ y_{t_A} = r \cdot \sin(\omega_s \cdot (t_A - \Delta_t)) \\ y_{t_A} = \left(x_{t_A} - x_{O_i}^{t_B}\right) \cdot \tan(\omega_s \cdot {}^s t_B) \end{cases} \tag{48}$$

The relationship between t_A and t_B can be obtained by solving Eq. (48) using MATLAB. Substitute it into Eqs. (43), (44), and (45), then the final model of center-to-center distance between adjacent two grooves is developed. It can be seen that h is a function of grinding parameters and ultrasonic vibration parameters. Then, the expected values of h and h^2 can be calculated using numerical solution of h.

The simulation test is conducted using MATLAB under certain conditions in Table 2.

Table 2 Simulation test parameters

Parameter	A (μm)	f (kHz)	n (r/min)	v_w (μm/s)	R (μm)
Value	6.5	20	9×10^3	100	1500

The simulation result of the instantaneous abrasive cutting thickness about t_A in several ultrasonic cycles is shown in Fig. 6. A positive h value indicates that the abrasive cuts into unmachined materials. A negative h value also indicates the abrasive withdraws from unmachined materials. It can be seen that h repetitively oscillates as analogous sine wave at ultrasonic frequency, which indicates that intermittent cutting is achieved in UAMEG from the view of single abrasive, and the average value of h is to be cut down significantly.

2 Experimental details

A comprehensive model for the quantitative prediction of surface roughness is presented, as given by Eq. (38). In order to predict the developed model of surface roughness effectively, the experiment of silica glass UAMEG is conducted using a set of self-assembled microgrinding machine tool, as shown in Fig. 7. The same levels of grinding depth given in Table 3 are adopted. The wheel feed is 100 μm. The other simulation and grinding experimental conditions are shown in Table 3. The microwheel is electroplated CBN grinding wheel with diameter of 3 mm and grit number of 230~270. Dimension of the silica glass sample is 50×20×3 mm.

Surface roughness measurements are conducted using Talysurf PGI surface coarseness profiling instruments. The resolution of surface roughness-measuring instrument is 0.8 nm. This means that the 0.8 nm is the minimum value of surface roughness that can be measured by the surface roughness-measuring instrument,

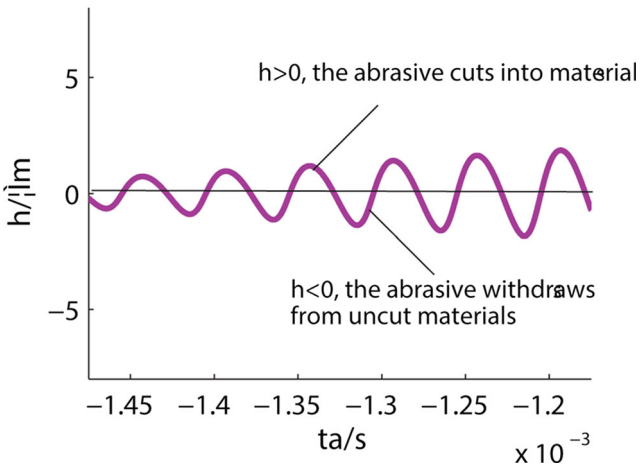

Fig. 6 Instantaneous abrasive cutting thickness (h) about t during half a wheel rotating cycle

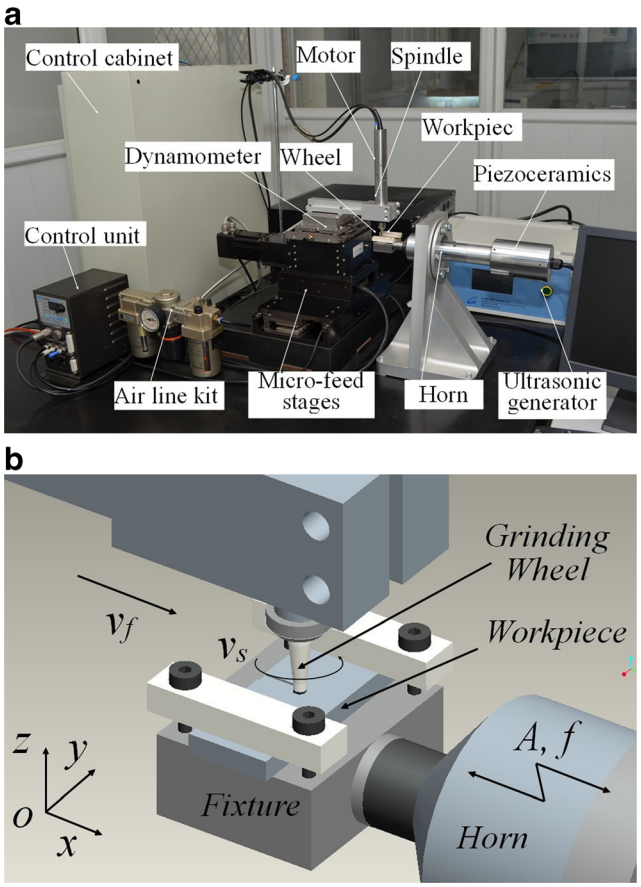

Fig. 7 Machine tool setup. **a** Picture of whole construction. **b** Amplified drawings

which is much smaller than the measured surface roughness in this work. So, measurements made by this instrument could be considered accurate enough for the present study. In addition, a Hitachi S-4800 field emission scanning electron microscope is used to generate the micrographs for this study.

3 Experimental results and discussion

3.1 Evaluation of θ

The value of θ plays a major role in predicting the surface quality. In order to use the model effectively, the value of θ

Table 3 Parameters of experiments

Experiment no.	A (μm)	n (r/min)	a_p (μm)	R_a	θ (deg)
1	8.5	18,000	1	0.0982	69.99
2	8.5	18,000	1.5	0.1029	56.86
3	8.5	18,000	2	0.2030	43.38
4	8.5	18,000	2.5	0.3690	33.78

must be evaluated. Calculation results of θ are shown in Table 3. It can be seen that the value of θ is severely influenced by grinding depth. It can be explained by the deficiency of triangular-groove-shaped assumption. With grinding depth increasing, the calculation value of θ decreases gradually. This tendency matches well with the result of Agarwal's study [12], which demonstrates that the predicted values of surface roughness using the circular-groove-assumed model fit the experimental results better than using the triangular-groove-assumed model. Thus, in order to effectively predict surface roughness in this work, value of θ corresponding to certain grinding depth is adopted for simulation.

3.2 Model verification

A series of verification experiments are conducted under different levels of ultrasonic amplitudes, wheel speeds, and grinding depths. Measured values of surfaces roughness of workpiece surfaces processed in UAMEG corresponding to certain conditions are shown in Table 4. In addition, the calculated values of $E(h)$ and $E(h^2)$ are listed in Table 4. Due to the calculated values of $E(h)$ and $E(h^2)$ are small by using MATLAB, the impact on this model is little, so the calculated value multiplied by a coefficient k. After calculation, the coefficient is equal to 250. Then, substituting the values of $E(h)$ and $E(h^2)$, surface roughness under each experimental condition is calculated using the surface roughness model given by Eq. (37).

From Fig. 8a, it can be seen that both experimental value and predicted value of surface roughness significantly decrease by about 50 % with assistance of ultrasonic vibration compared with conventional microgrinding. With ultrasonic amplitude increases from 6.5 to 8.5 μm, the surface roughness of both experiments and predictions decline gradually and tend to be steady.

As shown in Fig. 8b, the experimental value and predicted value of surface roughness show an decrease with wheel rotation speed growing from 8000 to 36,000 n/min. The experimental results of surface roughness decease more slightly with increase of wheel speed compared with simulation results.

As can be seen from Fig. 8c, workpiece surface roughness both experimentally measured and modeling predicted rise significantly—nearly tripled with grinding depth grows from 1 to 2.5 μm. And the upward trend of surface roughness accelerates with increasing of grinding depth.

It is indicated from Fig. 8 that large predictive values of surface roughness are larger than those experimental values measured under the conditions listed in Table 4. This may be due to that only two adjacent grooves are considered to characterize overlapping effect during surface roughness model development. Overlapping of grooves contributes decrease of surface roughness. However, in actual process of UAMEG, the overlapping effect is more complicated and significant due to reiteratively grain-workpiece interaction of all the abrasives on wheel end face. So, the experimentally measured results of surface roughness tend to be smaller than those predicted by the model developed in this work.

3.3 Analysis based on surface microstructure

In Fig. 9a, the darkness region represents complex fracture in surface material. It is indicative of brittle-regime removal and severe surface damage. It points to the fact that cracks pene trated into the final machined surface that lead to complex fracture in conventional micro end grinding under high instantaneous abrasive cutting thickness and undeformed chip thickness. Contrast result in UAMEG is shown in Fig. 9b. Squamous structures are formed on machined surface under ultrasonic assistance with amplitude of 6.5 μm, which indicates a complex process of brittle and ductile removal. It can be interpreted that intermittent cutting due to assisted ultrasonic vibration leads to the decrease of instantaneous abrasive cutting thickness and undeformed chip thickness. As is investigated above, instantaneous abrasive cutting thickness

Table 4 Surface roughness of experiments and prediction

Experiment no.	A (μm)	n (r/min)	a_p (μm)	$E(h)$	$E(h^2)$	R_a (μm) experiment	R_a (μm) prediction
1	8.5	18,000	1	0.803	0.647	0.0982	0.0741
2	8.5	18,000	1.5	0.803	0.647	0.1029	0.1254
3	8.5	18,000	2	0.803	0.647	0.2030	0.2053
4	8.5	18,000	2.5	0.803	0.647	0.3690	0.2796
5	7.5	18,000	2	0.906	0.821	0.2096	0.2378
6	6.5	18,000	2	1.025	1.144	0.2199	0.2884
7	0	18,000	2	1.675	2.781	0.5575	0.5512
8	8.5	8,000	2	1.215	1.476	0.2219	0.3493
9	8.5	27,000	2	0.675	0.456	0.1783	0.1676
10	8.5	36,000	2	0.375	0.141	0.1372	0.0936

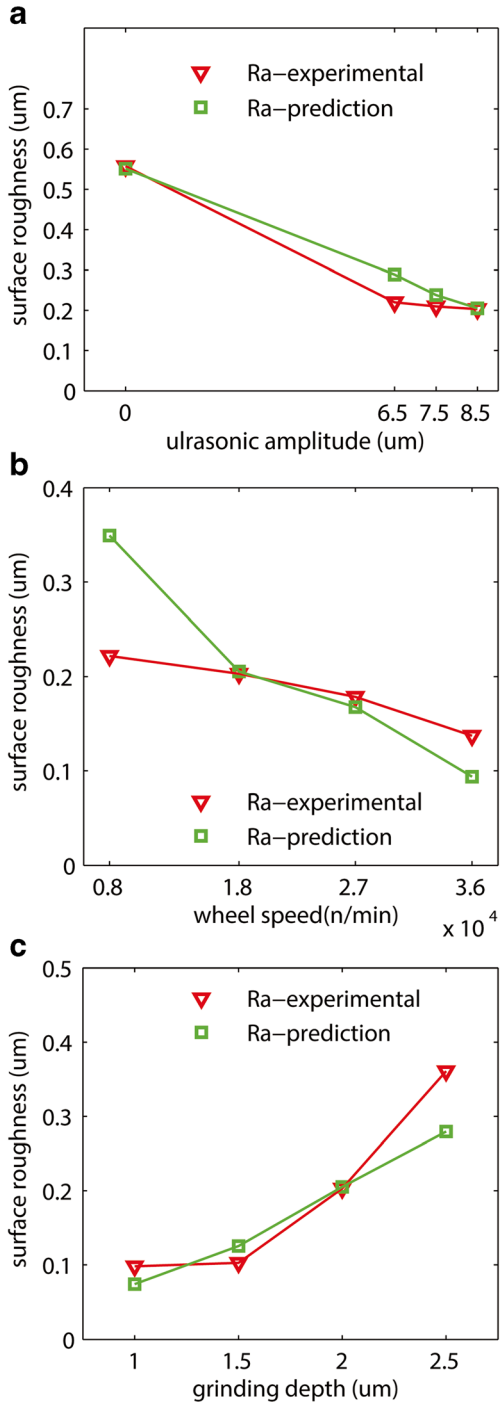

Fig. 8 Surface roughness presented at various values of grinding depth, wheel speed, and ultrasonic amplitude

repetitively oscillates as analogous sine wave at ultrasonic frequency. When the instantaneous abrasive cutting thickness increases from zero, material removal in the form of plastic deformation, meanwhile, the plastic deformation accumulates and enlarges with the instantaneous abrasive cutting thickness increasing. When the maximum undeformed chip thickness is more than the critical value t_c, cracks initiate and grow. As the instantaneous abrasive cutting thickness exceeds the critical value h_c, cracks achieve to the final machined surface. However, surface damage and surface roughness are significantly improved due to ultrasonic assistance.

The comparison between the characteristic of surface in Fig. 9b–d shows the influence of ultrasonic amplitude on machined surface. It can be seen that when the ultrasonic amplitude increases from 6.5 to 7.5 μm, there exists little evidence of fracture crack remaining on surface. It can be explained that ultrasonic effect becomes more significant with ultrasonic amplitude increasing. But when the ultrasonic amplitude increases to 8.5 μm, fracture cracks occur again and become even more severe than that in Fig. 9b, as shown in Fig. 9d. This may be due to the excessive impact power between the abrasive and materials when the ultrasonic amplitude increases to 8.5 μm.

When the grinding depth decreases from 2 to 1 μm, as is shown in Fig. 9d, e, a squamous structure takes the place of fracture on machined surface. It indicates that more material is removed in ductile region and the remaining fracture cracks are reduced with lower grinding depth.

Comparing Fig. 9d and f, it can be seen that machined surface is improved with the wheel speed increasing from 18,000 to 27,000 r/min. Obvious plastic ploughing grooves and trivial fractures are observed on the surface in Fig. 9f, which indicates that abrasive cutting thickness and undeformed chip thickness decline with the increase of wheel speed, and thus, brittle fracture is significantly reduced.

In conclusion, adding ultrasonic vibration can significantly improve the quality of machined surface due to intermittent cutting, which leads to the reduction of abrasive cutting thickness and undeformed chip thickness. But, ultrasonic vibration with excessive amplitude is disadvantageous for surface quality. Low grinding depth and high wheel speed are beneficial to the machined surface.

4 Conclusion

In this paper, an analytical model for surface roughness prediction is proposed to predict the surface roughness in UAMEG of silica glass, and the experimental study is conducted to finally establish and verify the proposed model. The conclusions are as follows:

(1) The model is based on the analysis of the grooves left by the grains that interact with the workpiece, which is characterized by the undeformed chip thickness. A geometric analysis based on a probabilistic approach is used to describe the arithmetic mean value, R_a. The relationship between the surface roughness and the undeformed chip thickness is found.

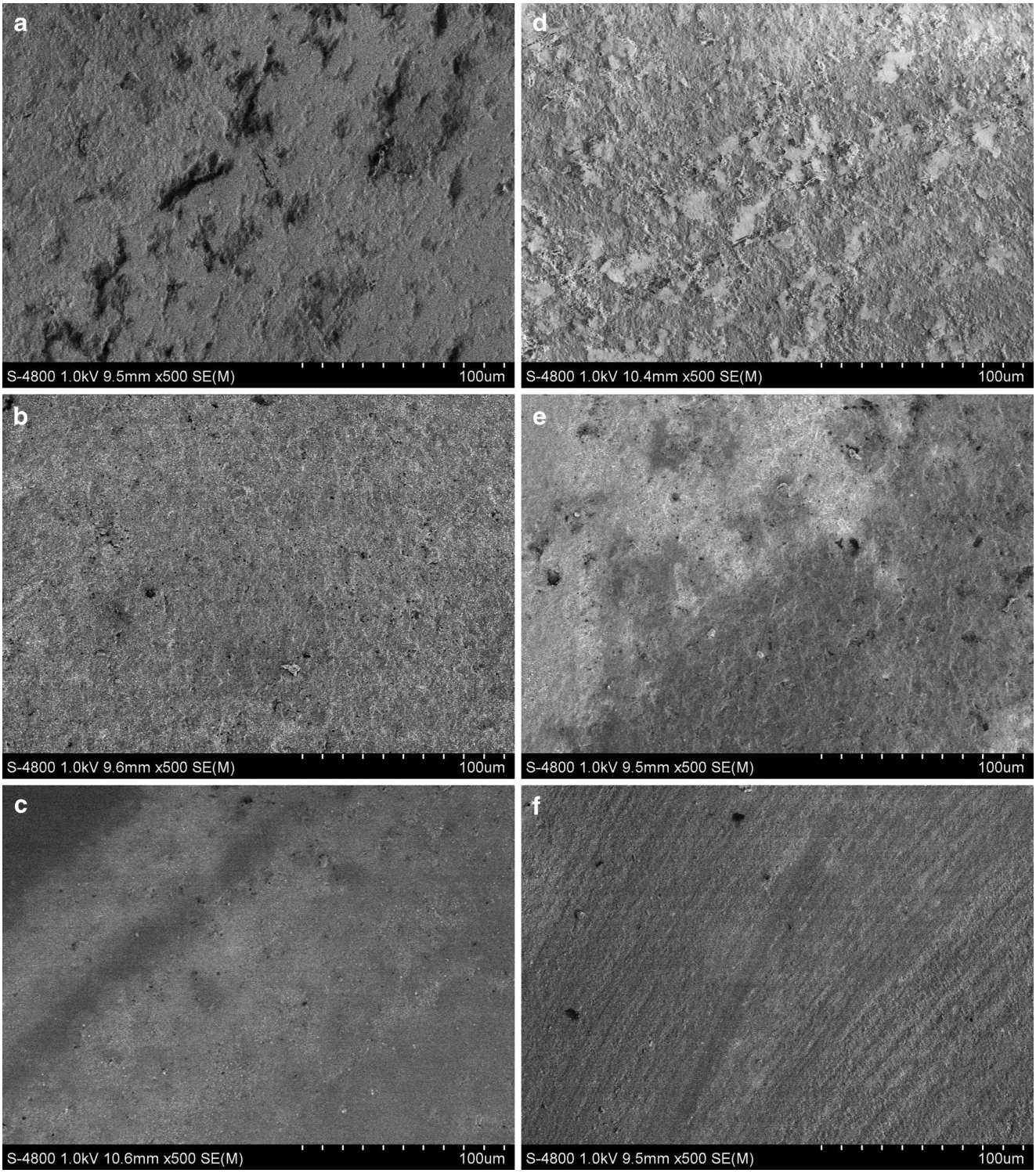

Fig. 9 Surface machined at **a** A=0 μm, a_p=2 μm, f_w=100 μm, n=18,000 r/min; **b** A=6.5 μm, a_p=2 μm, f_w=100 μm, n=18,000 r/min; **c** A=7.5 μm, a_p=2 μm, f_w=100 μm, n=18,000 r/min; **d** A=8.5 μm, a_p=2 μm, f_w=100 μm, n=18,000 r/min; **e** A=8.5 μm, a_p=1 μm, f_w=100 μm, n=18,000 r/min; and **f** A=8.5 μm, a_p=2 μm, f_w=100 μm, n=27,000 r/min

(2) The material properties, the wheel microstructure, the grinding conditions, etc. are included in the model. The model also incorporates the overlapping effect of grooves formed by the grains. By incorporating the overlapping effect, the model becomes more realistic.

(3) The effect of grinding parameters on the surface roughness is simulated and discussed. These grinding

parameters include grinding depth, wheel speed, and ultrasonic amplitude. The surface roughness increases with the increasing of grinding depth. The value of surface roughness is inversely proportional to ultrasonic amplitude and wheel speed. The predicted surface roughness shows a good agreement with experimental data.

Acknowledgments This work was supported by the Natural Science Foundation of Hebei Province of China (project numbers E2012202088 and E2012202112) and Innovation Fund for Outstanding Youth of Hebei University of Technology (project number 2012011).

Compliance with ethical standards The authors claim that none of the material in this paper has been published or is under consideration for publication elsewhere.

References

1. Masuzawa T (2000) State of the art of micromachining. CIRP Ann Manuf Technol 49:473–488
2. Brinksmeier E, Mutlugunes Y, Klocke F, Aurich JC, Shore P, Ohmori H (2010) Ultra-precision grinding. CIRP Ann Manuf Technol 59:652–671
3. Zhong ZW, Venkatesh VC (2009) Recent developments in grinding of advanced materials. Int J Adv Manuf Technol 41:468–480
4. Sreejith PSN (2001) Material removal mechanisms in precision machining of new materials. Int J Mach Tools Manuf 41:1831–1843
5. Liu K, Li XP, Liang SY (2007) The mechanism of ductile chip formation in cutting of brittle materials. Int J Adv Manuf Technol 33:875–884
6. Gan J, Wang X, Zhou M, Ngoi B, Zhong Z (2003) Ultraprecision diamond turning of glass with ultrasonic vibration. Int J Adv Manuf Technol 21:952–955
7. Tawakoli T, Azarhoushang B, Rabiey M (2009) Ultrasonic assisted dry grinding of 42CrMo4. Int J Adv Manuf Technol 42:883–891
8. Tawakoli TAB (2008) Influence of ultrasonic vibrations on dry grinding of soft steel. Int J Mach Tools Manuf 48:1585–1591
9. Chen HF, Tang JY, Zhou W (2013) An experimental study of the effects of ultrasonic vibration on grinding surface roughness of C45 carbon steel. Int J Adv Manuf Technol 68:2095–2098
10. Yan YY, Zhao B, Liu JL (2009) Ultraprecision surface finishing of nano-ZrO2 ceramics using two-dimensional ultrasonic assisted grinding. Int J Adv Manuf Technol 43(5–6):462–467
11. Prasanna MM, Miehele HM (2014) Force and thermal effects in vibration-assisted grinding. Int J Adv Manuf Technol 71:1117–1122
12. Wang Y, Lin B, Wang SL, Cao XY (2014) Study on the system matching of ultrasonic vibration assisted grinding for hard and brittle materials processing. Int J Mach Tools Manuf 77:66–73
13. Jianhua Z, Yan Z, Shuo Z, Fuqiang T, Lanshen G, Ruizhen D (2014) Study on effect of ultrasonic vibration on grinding force and surface quality in ultrasonic assisted micro end grinding of silica glass. SHOCK VIB 2014:1–10
14. Hecker RL, Liang SY (2003) Predictive modeling of surface roughness in grinding. Int J Mach Tools Manuf 43:755–761
15. Agarwal S, Rao PV (2005) A probabilistic approach to predict surface roughness in ceramic grinding. Int J Mach Tools Manuf 45:609–616
16. Agarwal S, Venkateswara P, Rao (2010) Modeling and prediction of surface roughness in ceramic grinding. Int J Mach Tools Manuf 50:1065–1076
17. Gao GF, Zhao B, Xiang DH, Kong QH (2009) Research on the surface characteristics in ultrasonic grinding nano-zirconia ceramics. J Mater Process Technol 209:32–37
18. Gopal AV, Rao PV (2004) A new chip-thickness model for performance assessment of silicon carbide grinding. Int J Adv Manuf Technol 24:816–820
19. Younis MA, Alawi H (1984) Probabilistic analysis of the surface grinding process. T Can Soc Mech Eng 8:208–213
20. Park HW (2008) Development of micro-grinding mechanics and machine tools, Georgia Institute of Technology